



1 **A Consolidated Database of Mercury Observations for Permafrost Regions**

2 Christine L. Olson¹, Kevin Schaefer¹, Alyssa Azaroff², H el ene Angot³, Thomas A. Douglas⁴,
3 Maria Florencia Fahnestock⁵, Charlotte Haugk², Gustaf Hugelius², Erfan Jahangir³, Sofi
4 Jonsson², Adam Kirkwood⁶, Jennifer Korosi⁷, Mina Nasr^{8,9}, David Olefeldt¹⁰, Connor
5 Olson^{1,11}, Laura Sereni³, Sarah Shakil¹², Kyra St. Pierre¹³, Lauren Thompson¹⁰, and Scott
6 Zolkos¹⁴.

7 ¹ University of Colorado, Boulder, USA

8 ² Stockholm University, Sweden

9 ³ Univ. Grenoble Alpes, CNRS, INRAE, IRD, Grenoble INP, IGE, Grenoble, France

10 ⁴ U.S. Army Cold Regions Research and Engineering Laboratory Fort Wainwright, Alaska, USA

11 ⁵ University of New Hampshire, USA

12 ⁶ Carleton University, Canada

13 ⁷ York University, Canada

14 ⁸ Env. And Protected Areas, Gov. of Alberta, Canada

15 ⁹ University of Calgary, Department of Geography

16 ¹⁰ Department of Renewable Resources, University of Alberta, Edmonton, Alberta, Canada

17 ¹¹ Harvard University, USA

18 ¹² Uppsala University, Sweden

19 ¹³ University of Ottawa, Canada

20 ¹⁴ Woodwell Climate Research Center, USA

21

22 **E-mail:** christine.olson@colorado.edu, kevin.schaefer@colorado.edu

23 **Keywords:** mercury (Hg), PermHg database, permafrost, soil, water, vegetation, lake sediment

24

25 **Abstract**

26 Permafrost soils are one of the largest terrestrial pools of mercury (Hg) in the world, storing an
27 estimated 500–1500 Gg of Hg in the top three meters of soil. Ongoing climate-driven thaw
28 threatens to release this legacy Hg into the environment. Efforts to quantify and model this pool
29 have been hindered by a lack of harmonized, spatially resolved observations. To address this, we
30 compiled a database of 117,802 Hg observations collected between 1988 and 2022 from 59
31 studies across Arctic, sub-Arctic, and alpine permafrost regions of the Northern Hemisphere,



32 including North America, northern Europe, Eurasian and the Tibetan Plateau. The database
33 includes Hg concentration measurements in solid materials—such as soil, leaves, roots, wood,
34 and litter—as well as in water samples from soil porewater, lakes, and rivers across the northern
35 hemisphere permafrost domain. The database enables cross-site synthesis, model calibration and
36 evaluation, and environmental assessments by standardizing and harmonizing data from diverse
37 sources. Data harmonization steps included unit conversion, categorization of observations by
38 type, and quality control measures to ensure consistency across studies. Analytical uncertainty
39 was preserved where reported in source studies, and qualitative uncertainty indicators and flags
40 were applied where uncertainty information was incomplete or heterogeneous. Mercury
41 concentrations vary widely across observations, with lake sediment showing the highest median
42 values (70 ng g⁻¹, IQR: 45-116), followed by soil (50 ng g⁻¹, IQR: 32-90), and vegetation (15 ng
43 g⁻¹, IQR: 9-33). Water observations had a median of 2 ng L⁻¹ (IQR: 2-6). Statistically significant
44 differences in Hg concentrations among observation types were observed at both global and
45 regional scales, consistently following the pattern: lake sediment > soil > vegetation. These
46 patterns, along with spatial and observation-type biases, highlight the need for improved
47 coverage in underrepresented regions such as Eurasia. The database is freely accessible through
48 Zenodo under the concept DOI 10.5281/zenodo.18300989 (all versions), to support ongoing
49 research and model development in Arctic and sub-Arctic Hg cycle studies.

50 **1. Introduction**

51 Permafrost soils also contain the largest terrestrial pool of Hg in the world (Schuster et al.,
52 2018; Olson et al., 2018; Lim et al., 2020). Anthropogenic activities and natural sources such as
53 volcanoes and rock weathering release Hg into the environment. Mercury in permafrost
54 primarily originates from long-range atmospheric transport of Hg from lower latitudes (Dastoor
55 et al., 2022). About two-thirds of Hg in remote permafrost regions is deposited to terrestrial
56 ecosystems where it accumulates in soils via vegetation uptake and transfer through litterfall and
57 throughfall (Obrist et al., 2017; Olson et al., 2018, 2019). As permafrost thaws, Hg bound to
58 organic rich matter may become mobilized into terrestrial and aquatic ecosystems (Chételat et
59 al., 2022; Jonsson et al., 2022; St. Pierre et al., 2018). Once mobilized, it can be transported to
60 wetlands, rivers (Fabre et al., 2024; Zolkos et al., 2020), lakes (MacMillan et al., 2015; Varty et
61 al., 2021), and coastal (Giest et al., 2025) environments where microbial processes can convert it
62 to methylmercury (MeHg) – a highly toxic and bioaccumulative form (Jonsson et al., 2022). As



63 climate warming accelerates, this sequence of thaw-driven mobilization, transport, and
64 methylation could trigger a permafrost–Hg feedback with far-reaching implications for
65 ecosystem and human health, particularly for Arctic and sub-Arctic communities reliant on
66 aquatic foods as a dietary staple (Schaefer et al., 2020; Basu et al., 2022; Gartler et al., 2025).
67 Understanding the complete terrestrial Hg budget—including vegetation-mediated inputs —is
68 critical for projecting how climate change will alter global Hg cycling.

69 Permafrost regions play a critical role in regulating both local and global Hg cycling. Despite
70 its importance, observational data from these regions remain spatially limited and are rarely
71 synthesized across media (e.g., soil, vegetation, water sediments). As a result, many global Hg
72 budgets either exclude these areas or rely on highly uncertain estimates (Outridge et al., 2018;
73 Sonke et al., 2023; Zhang et al., 2023). Although measurements exist, they are dispersed in the
74 literature and have not been integrated into forms usable for larger-scale modeling or policy
75 assessments. Current global budgets incorporate detailed estimates of anthropogenic and natural
76 emissions, wet and dry deposition fluxes, and reservoirs in the ocean, land, and vegetation, yet
77 cold-region biogeochemistry and permafrost processes are inadequately represented. An
78 improved understanding of the global Hg cycle—especially in permafrost—is critical to our
79 understanding of the global Hg cycle and to effectively monitor reduction efforts under
80 international frameworks such as the Minamata Convention on Mercury. An integrated database
81 of available Hg observations in permafrost regions is needed to better represent this outsized
82 global pool.

83 Mercury measurements in permafrost regions remain spatially limited, fragmented across
84 observation types, and largely unintegrated across studies (Arctic Monitoring and Assessment
85 Programme, 2022). Permafrost soil inventories vary widely – from 500-1500 Gg of Hg in the top
86 three meters of soil—due to sparse and spatially unevenly distributed measurements (Schuster et
87 al., 2018; Olson et al., 2018; Lim et al., 2020). Large-scale extrapolations like these rely on the
88 upscaling of localized data using carbon content and Hg-to-carbon ratios from a few accessible
89 regions, leading to geographic biases in global estimates (Lim et al. 2020). In addition,
90 insufficient stratification of observations by ecosystem or soil type (e.g., organic vs. mineral
91 soils) limits the accuracy of Hg storage estimates and the ability to capture spatial heterogeneity.
92 Expanding observational coverage across permafrost regions and ensuring representation across



93 key soil types in permafrost regions are essential to constrain these estimates and reduce
94 uncertainty. Vegetation measurements are even more rare and not co-located with soil Hg
95 measurements, despite vegetation being a key pathway for Hg deposition and transfer to soils
96 through litterfall and wood decomposition. This process plays a crucial role in the accumulation
97 of Hg in permafrost over time, as plant-derived organic matter—and its associated Hg—is buried
98 and frozen. Without co-located vegetation and soil measurements, it is difficult to reconstruct
99 historical Hg inputs and constrain the drivers of current permafrost Hg inventories. Aquatic
100 systems are another critical component, acting as downstream receptors of Hg mobilized from
101 thawing permafrost. In these environments, certain conditions promote the microbial conversion
102 of inorganic Hg to MeHg—a potent neurotoxin that bioaccumulates in food webs and poses the
103 greatest risk to wildlife and human health. Distinct methylation hotspots have been identified in
104 wetlands (Thompson et al., 2025), ponds (MacMillan et al., 2015), and lakes (Jonsson et al.,
105 2022); however, limited data on Hg inputs and outputs hinders our ability to quantify fluxes and
106 establish clear linkages with surrounding terrestrial sources. In permafrost regions, rivers such as
107 the Yukon, Mackenzie, and Ob show high seasonal variability in Hg fluxes, peaking during
108 spring thaw and snowmelt (Sonke et al., 2018; Zolkos et al., 2020). Exports of Hg from streams
109 and rivers in permafrost are sparse and vary widely, driven by differences in land cover, geology,
110 and watershed complexity. This lack of integrated data across observation types hinders our
111 ability to predict future ecological impacts and to quantify the growing contribution of thawing
112 permafrost Hg to the global budget. Consolidating existing observations is therefore a critical
113 first step towards improving predictive models, monitoring strategies, and broader scientific
114 analyses (Horsburgh et al., 2009).

115 This paper introduces the PemHg database, developed through an extensive effort to compile,
116 standardize, and harmonize Hg observations from permafrost-affected environments. The
117 database includes both published and unpublished data on Hg concentrations in soil, aquatic
118 systems, and vegetation across permafrost regions. The goal is to support synthesis efforts,
119 model development, and risk assessment. By improving access to Hg observations in cold-
120 region systems, the PermHg database provides a robust, centralized platform that can be used to
121 enhance our understanding of permafrost landscapes and to help identify implications for
122 northern high-latitude ecosystems.



123

124 **2. Methods**

125 We compiled Hg observations by surveying peer-reviewed literature via Web of Science and
126 other scholarly databases, supplemental materials, and open-access data repositories, as well as
127 incorporating unpublished measurements contributed directly by collaborating researchers. The
128 PermHg database is the result of numerous research groups from around the world combining
129 original measurements collected in permafrost regions. We sought to prioritize primary
130 observations, although some observations are from prior synthesis papers. All nomenclature,
131 units, and formats were standardized into a single harmonized database for general use. While
132 the database is comprehensive, its completeness is limited by geographic bias in the published
133 record, variable reporting standards, and uneven coverage across ecosystem types. Descriptions
134 of observation types, standardization procedures, and methodologies are detailed below. This
135 will be one of the first open sources, integrated global permafrost Hg databases combining soil,
136 sediment, aquatic systems, and vegetation observations on a large scale.

137 In addition to primary literature sources, a subset of soil permafrost mercury observations
138 was sourced from an independently curated database developed by the Bolin Centre for Climate
139 Research (DOI: XXX; A permanent DOI will be assigned upon acceptance/publication). These
140 data are archived separately and contribute harmonized permafrost mercury observations and
141 associated metadata that complement the broader PermHg compilation.

142

143 **2.1. Study Area**

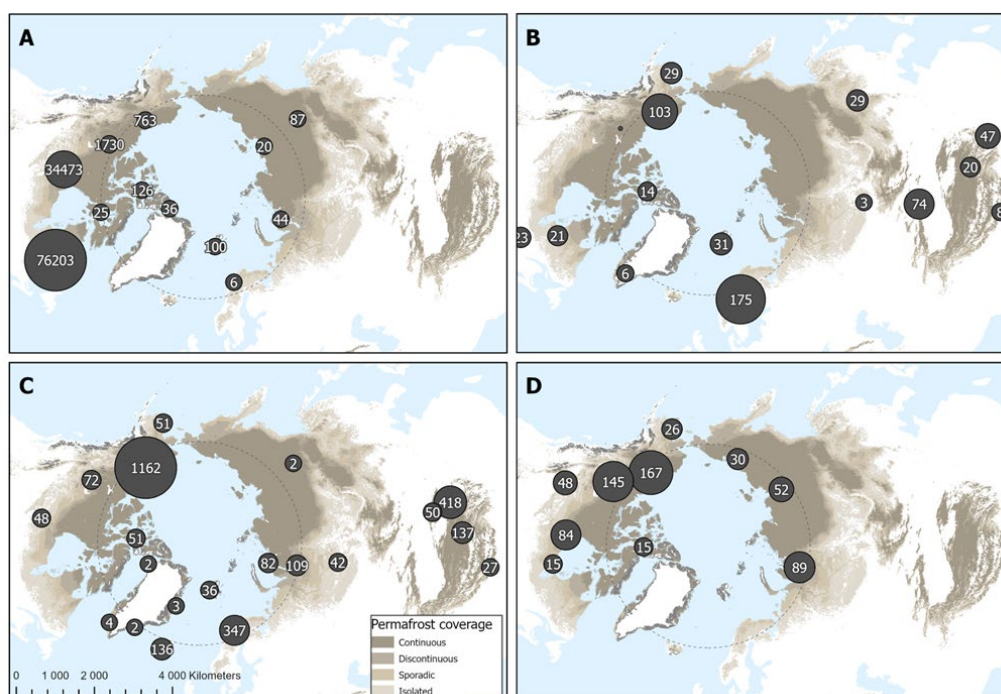
144 The database includes observations from Arctic, sub-Arctic, and alpine permafrost
145 regions in the Northern Hemisphere, including the Tibetan Plateau. Site selection was based on
146 geographic and climatic criteria guided by the modeled permafrost extent and ground
147 temperature map of Obu et al. (2019a). Specifically, we included areas with a permafrost
148 probability of $\geq 10\%$ or greater and mean annual ground temperature below 0°C , capturing a range
149 of permafrost zones from continuous to isolated (Obu et al., 2019a).

150 Vegetation cover types for plant Hg data were classified using the circumpolar vegetation
151 map from the ABCflux database (Virkkala et al., 2022). These include land cover classes such as



152 mixed and needleleaf forests, boreal and tundra wetlands, and shrub and barren tundra.
153 Observation locations were overlain on the land cover map to assign the dominant vegetation
154 type for each observation. This enables grouping of observations by ecosystem, which may aid in
155 identifying Hg uptake patterns across different environmental conditions. Note that spatial
156 resolution of the land cover database may be limited in some areas; however, using a
157 standardized land cover supports future ecological comparisons and model parameterization
158 efforts.

159 A map of the geographic domain is provided in **Fig. 1** to visualize the spatial distribution
160 of data points and overall coverage of the study. The figure includes a map of Hg observations,
161 with spatial coverage differentiated by observation type. Circle size and embedded numbers
162 indicate observation density, while circle color indicates observation type (e.g., soil, water,
163 vegetation, or lake sediment). The background shading represents the likelihood of permafrost
164 occurrence, based on the probabilistic map from Obu et al. (2019b).



165

166 **Figure 1.** The map shows the global PermHg observation locations for (a), lake sediment, (b) vegetation
167 (c) soil and (d) water. Water data includes observations in lakes, rivers, creeks, oceans, wetlands, ponds,



168 and soil porewater. Circle size and numbers show observation density or counts per area. The
169 background shading shows the probability of different types of permafrost based on criteria defined in
170 Obu et al., 2019. Permafrost is classified by probability: continuous (>0.9), discontinuous (0.5–0.9),
171 sporadic (0.1–0.5), and isolated patches (0.001–0.1). These categories, shown in varying shades of
172 brown, indicate the likelihood that permafrost is present at a given location.

173

174 **2.2. Data Description**

175 We focused on extracting Hg measurements from environmental compartments most
176 relevant to the terrestrial biosphere and Hg cycling models including soil, lake sediment, water,
177 and vegetation. Water data includes observations in lakes, rivers, creeks, oceans, wetlands,
178 ponds, and soil porewater. All observations include the following metadata: the original
179 observation identifier if available, site name, country, sample number, date of collection,
180 laboratory, contact name, contact email, paper identifier, latitude and longitude, measurement
181 instrument, total Hg concentration, total Hg measurement error, notes, collector, range flag, and
182 outlier flag. A “ReadMe tab” is included on Zenodo ([10.5281/zenodo.18300989](https://doi.org/10.5281/zenodo.18300989), concept DOI)
183 for each database type, providing detailed descriptions of all column variables and units (Olson
184 et al., 2026). Additional metadata specific to the observation type is detailed in the following
185 paragraphs.

186 Soil data include available information on soil type, horizon, vegetation type, sample
187 depth, bulk density, loss-on-ignition (LOI; as a proxy for organic matter), soil organic carbon
188 content, hg-to-carbon ratio, and volumetric water content. Soil horizon and depth information
189 help distinguish surface organic layers from mineral soils, which can be markedly different in Hg
190 concentration (Lim et al., 2020). Bulk soil density and organic carbon (OC) measurements are
191 used to calculate Hg stocks, and pairing Hg with OC enables upscaling across permafrost regions
192 where OC data are widely available. LOI provides a complementary proxy for total organic
193 matter, helping to capture variability in Hg–organic matter associations. Volumetric water
194 contents are helpful for determining MeHg production potential and possibly redox states.
195 Collectively, these parameters support assessment of Hg partitioning, transportation, and
196 transformation.



197 Lake sediment data provides a long-term archive of Hg deposition and accumulation,
198 capturing both historical and more recently derived inputs. Surface sediments are also an
199 important site of Hg methylation and are critical to understanding Hg loading to aquatic food
200 webs. Lake sediment data includes information on sampling location and context, such as soil
201 type (for porewater samples), vegetation type, location description, catchment size, wetland
202 cover, depth of sample, soil organic carbon, and Hg to carbon ratios. These metadata help us
203 interpret how Hg is retained or transported, potential Hg sources, methylation potential, and
204 deposition timeline.

205 Water data includes observations in lakes, rivers, creeks, oceans, wetlands, ponds, and
206 soil porewater. Water data also includes information on sampling location of the catchments
207 such as soil type (for porewater observations), vegetation type, site description, catchment size,
208 wetland cover, depth of sample, dissolved Hg concentration, MeHg concentration, total organic
209 carbon, dissolved organic carbon, Hg to carbon ratio, turbidity, pH, electrical conductivity,
210 alkalinity, total phosphorus, chloride, sulfate, and total dissolved solids. These water chemistry
211 measurements were included to help evaluate Hg concentrations and relevant processes in
212 aquatic systems including transformation, sources, mobility, bioavailability, binding, speciation,
213 and methylation.

214 Vegetation data include scientific and common species names, vegetation type, above
215 ground biomass, and sampled components such as leaves, roots, and woody tissue, including
216 tree-ring samples that can provide temporal records of Hg accumulation (Zhang et al., 1995;
217 Kang et al., 2022). Inclusion of these variables allows for comparison of Hg concentrations
218 across plant species functional types and environmental conditions. Tree-ring data are useful for
219 understanding historical trends in atmospheric Hg, allowing for records of Hg uptake over
220 decades to centuries. This is particularly helpful in remote regions, where long-term monitoring
221 is lacking.

222 Together, these metadata and Hg measurements provide critical context for
223 understanding Hg fate, transport, and transformation across various ecosystems. By
224 standardizing and compiling these parameters, the database enables cross-site comparison, model
225 development, and process-based investigations of Hg cycling in permafrost-affected landscapes.
226 While Hg measurements and location were the primary focus of this synthesis effort, we also



227 incorporated additional environmental parameters where available to support broader application
228 and interpretation.

229

230 **2.3. Data Harmonization and Standardization**

231 The database follows a standardized file and metadata structure, with clearly defined
232 columns, data types, and consistent formats for easy integration and use. Unit conversion was
233 applied to ensure all measurements are reported in standard units and maintain consistency
234 across studies. This includes ng g^{-1} dry weight for solids (soil, lake sediment, vegetation) and ng
235 L^{-1} for liquids (water). When uncertainty estimates were available, they were converted to the
236 same units. Latitude and longitude are reported in decimal degrees using the World Geodetic
237 System 1984 (WGS 84) coordinate reference system. The database includes core identifiers such
238 as site, location, and sample ID, collection date, laboratory name, contact person and email,
239 sample collector information, and additional notes relevant to data interpretation.

240 A uniform classification standard was implemented for vegetation observations. These
241 include vegetation type – the 12 vegetation classes defined in Virkkala et al. (2022), including
242 boreal wetland, mixed forest, deciduous needleleaf forest, evergreen forest, deciduous broadleaf
243 forest, sparse boreal vegetation, wetland tundra, shrub tundra, prostrate shrub tundra, graminoid
244 tundra, and barren tundra. If the vegetation type could not be distinguished, “NA” is reported.
245 The vegetation observations also contain a standardized “Component” column that specifies
246 whether the observations were moss, lichen, grass, root, leaf, needle, stem, twig, bole wood,
247 bark, or litterfall.

248 Missing metadata, such as unreported sample depths or inferred vegetation types, were
249 handled through reasonable assumptions based on available information and clearly flagged to
250 document associated uncertainty and ensure transparency. Missing data are reported as “NA” for
251 text cells and “-999” for numeric fields. The implications of these assumptions, variable
252 uncertainty reporting, and methodological heterogeneity across studies are further evaluated
253 through uncertainty indicators and validation checks described in Sect. 2.4.

254

255 **2.4 Uncertainty and Quality Control**



256 Uncertainty in the PermHg database arises primarily from heterogeneity in sampling
257 methods, analytical techniques, reporting standards, and metadata completeness across
258 contributing studies. Because the database compiles previously published observations rather
259 than generating new measurements, uncertainty characterization focuses on identifying potential
260 sources of variability and providing transparent indicators to support cautious interpretation,
261 rather than re-evaluating analytical accuracy.

262 Cross-study consistency and potential uncertainty were assessed using range checks and
263 statistical outlier flagging. Range flags are numerical indicators assigned to a data point based on
264 whether the values live within predefined minimum and maximum expected limits. For this
265 database, we use a conservative upper bound of 500 ng g⁻¹ for soil, lake sediment, and vegetation
266 observations and 100 ng L⁻¹ for water observations. Any observation above these values was
267 assigned a “1” in the range flag column and assumed to be outside of natural background values.
268 Observations that fell below these range flags were assigned a “0”. The threshold of 500 ng g⁻¹
269 for soils, lake sediments, and vegetation and 100 ng L⁻¹ for water observations was based on
270 published ranges of natural background concentrations observed in global and regional studies,
271 with values rarely exceeding this level outside of industrial or mining-impacted areas (Mei Lu et
272 al., 2016; Olson et al., 2022; Wohlgemuth et al., 2022). Any outlier exceeding three times the
273 interquartile range (difference between first and third quartile) was flagged and assigned a “1”.
274 All other values not exceeding 3xIQR were assigned “0”.

275 Analytical uncertainty was included for total Hg, MeHg, dissolved Hg, total organic
276 carbon, dissolved organic carbon, soil organic carbon, Hg to carbon ratio, volumetric water
277 content, and bulk density when such information was reported in the source studies. However,
278 uncertainty reporting was inconsistent across publications, and many observations lack explicit
279 error estimates or detection limits. As a result, uncertainty cannot be uniformly quantified across
280 the entire dataset. To address this limitation, qualitative uncertainty information and assumptions
281 made during data extraction (e.g., inferred coordinates or sample depths) were documented in a
282 notes field associated with each observation type to provide users with additional context
283 regarding potential sources of uncertainty or bias.

284 2.5 Data Analysis



285 We used several tools to analyze the PermHg database. To visualize the spatial distribution
286 and density of Hg observations globally, we used point clustering in ArcGIS Pro to generate
287 plots where observations were aggregated into circular clusters of varying size, with each circle
288 scaled to represent the number of observations within a given area. Boxplots were generated
289 using Python (version 3.13.3) with the Seaborn and Matplotlib libraries to visualize the
290 distribution of Hg concentrations across observation types and regions. Microsoft Excel was
291 used to generate column charts and explore the distribution of Hg concentrations across
292 observation types. Summary statistics, including count, mean, geometric mean, standard
293 deviation, first quartile (Q1), and third quartile (Q3), were calculated using built-in Excel
294 functions. These built-in functions provided a preliminary assessment of central tendency,
295 spread, and skewness within each observation type.

296 **3. Validation**

297 Validation of the PermHg database focuses on assessing internal coherence and plausibility
298 of the compiled observations rather than independent verification of individual measurements.
299 As the database aggregates previously published data, validation is based on consistency across
300 studies, agreement with established environmental patterns, and transparent documentation of
301 uncertainty and quality indicators (Sects. 2.3–2.4).

302 Across observation types and geographic subsets, the compiled data exhibit internally
303 consistent and environmentally plausible patterns. Summary statistics and distributional analyses
304 (Sect. 4; Figs. 2 and 4) show relative mercury concentrations among lake sediment, soil,
305 vegetation, and water that align with well-established mercury partitioning and accumulation
306 processes in terrestrial and aquatic systems (Section 2.4). No systematic contradictions or study-
307 level anomalies were identified that would indicate errors arising from data harmonization or
308 compilation.

309 Validation does not assess the analytical accuracy of individual measurements, which
310 remains the responsibility of the original studies. Instead, the combination of standardized data
311 structures, uncertainty indicators, range and outlier flags, and cross-study consistency supports
312 the use of the PermHg database for synthesis, comparative analyses, and model applications,
313 provided users account for documented limitations and uncertainty from each respective study.



314 4. Results

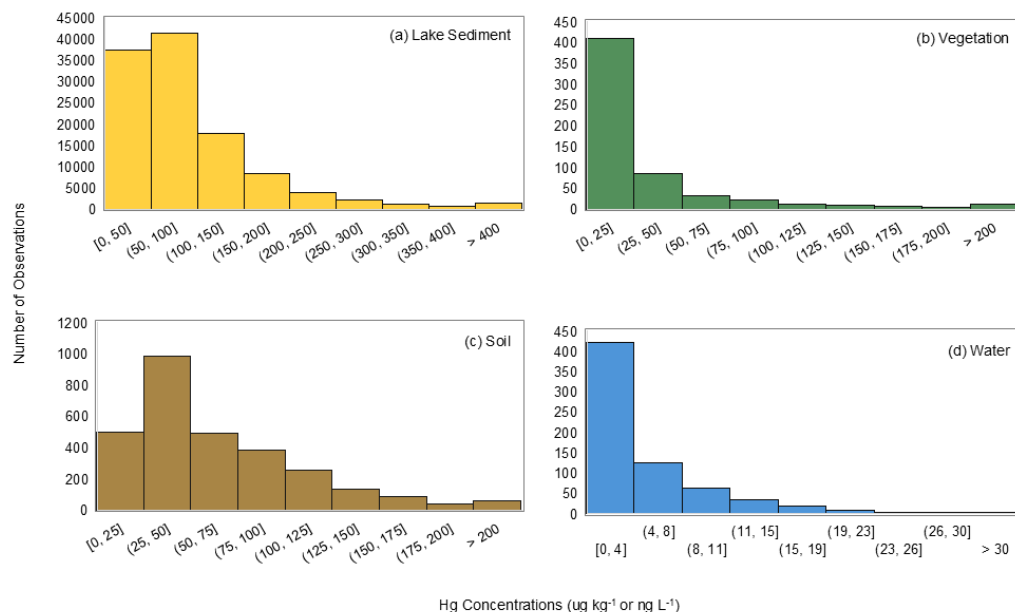
315 4.1. Data Summary

316 **Table 1** below details the observation count, median, geometric mean, standard
317 deviation, and upper and lower quartiles for each sample medium. These values highlight the
318 variability and distribution of Hg concentrations within each medium. A total of 31 papers were
319 included for the vegetation observations, four papers for the lake sediment observations, 17
320 papers for the soil observations, and 11 papers for the water observations. A small subset of
321 unpublished data was included for some observation types, comprising approximately 68
322 sediment observations and 75 water observations. The studies included in the database are
323 summarized in a table, with full citation details provided in Zenodo under the concept
324 DOI:10.5281/zenodo.18300989 (Olson et al., 2026).

325 **Table 1.** Summary statistics of Hg observations in permafrost-dominated regions including lake sediment
326 (ng g⁻¹), soil (ng g⁻¹), vegetation (ng g⁻¹), and water (ng L⁻¹). The minimum, 25th percentile, median, 75th
327 percentile, maximum, geometric mean, standard deviation, and count are included for each medium type.

| | Lake Sediment (ng g ⁻¹) | Soil (ng g ⁻¹) | Vegetation (ng g ⁻¹) | Water (ng L ⁻¹) |
|--------------------|-------------------------------------|----------------------------|----------------------------------|-----------------------------|
| Minimum | 1 | 1 | 1 | 0.0 |
| 25th Percentile | 45 | 32 | 9 | 1.5 |
| Median | 70 | 50 | 15 | 2.5 |
| 75th Percentile | 116 | 90 | 33 | 5.9 |
| Maximum | 9820 | 503 | 400 | 32.6 |
| Geometric Mean | 71 | 48 | 17 | 2.0 |
| Standard Deviation | 118 | 48 | 51 | 5.0 |
| Count | 113613 | 2923 | 590 | 676 |

328
329 Mercury concentrations across the four observation types—lake sediment, soil, vegetation, and
330 water—displayed predominantly left-skewed distributions (**Fig. 2**). Lake sediment and soil
331 observations showed higher median Hg concentrations compared to vegetation and water,
332 consistent with their roles as primary Hg reservoirs. Vegetation exhibited the lowest
333 concentrations overall, while water Hg concentrations, though generally low, spanned a
334 relatively wide range. The skewness in all matrices highlights that low-to-moderate
335 concentration observations are more common than extreme high values.



336

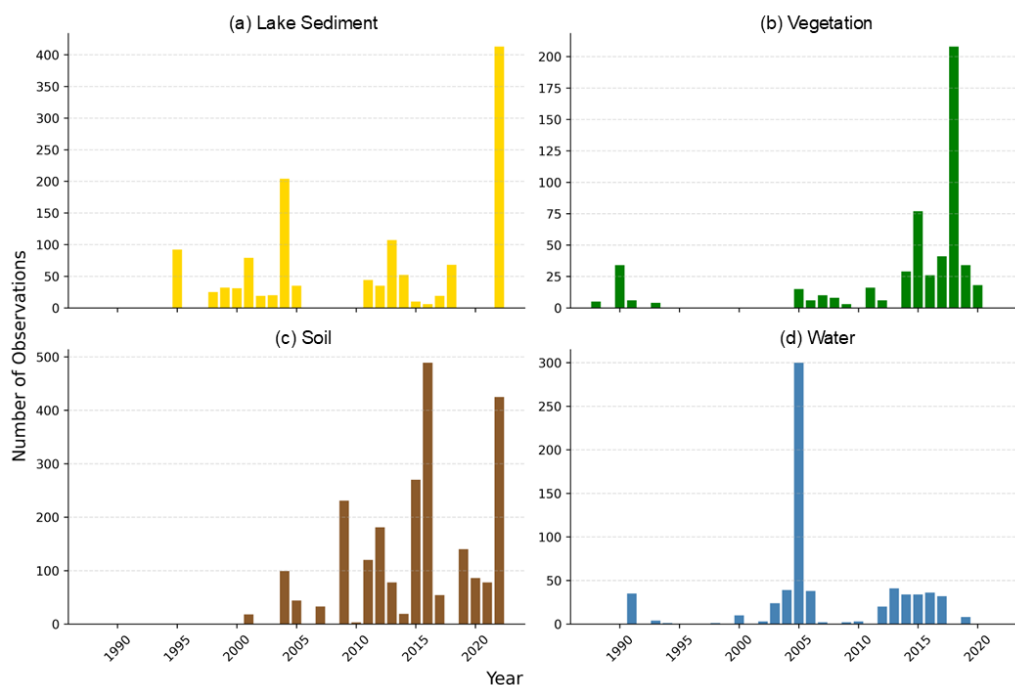
337 **Figure 2.** Histogram distributions of mercury concentrations in (a) lake sediment, (b) vegetation, (c) soil,
338 and (d) water. All matrices show left-skewed distributions, with lake sediment and soil exhibiting higher
339 median concentrations than vegetation and water. Water concentrations are plotted on a separate y-axis
340 scale to accommodate lower values relative to solid matrices.

341

342 **Figure 1** shows the geographic distribution of data points on a global map, illustrating
343 the spatial spread of measurements across the study region. Circle size and numbers within the
344 circles show observation density. Lake sediment observations are largely concentrated in
345 Canada, particularly towards the eastern side of the country. Some lake sediment observations
346 also occurred in the Canadian Arctic Archipelago and northern Russia. Vegetation observations
347 are concentrated in central Alaska, the Tibetan Plateau, and northern Europe. Some vegetation
348 observations are also visible in northern China, Greenland, Russia, and Canada. Soil
349 observations are highly concentrated in Alaska, the Tibetan Plateau, western Canada and
350 northern Europe, with clusters also existing in western Russia and the Rocky Mountains of the
351 United States. Water observations were the sparsest, with sampling clustered in the north slope
352 of Alaska and along major Arctic Rivers—the Ob, Mackenzie, Yukon, Lena, and Kolyma. Some
353 water observations are also present in the Hudson Bay of Canada.



354 The temporal distribution of Hg observations in the PermHg database is shown in **Fig. 3**,
355 highlighting the years in which samples were collected for each observation type. Lake sediment
356 observations span from 1995 to 2022, with notable peaks in sampling effort in 2004 and again in
357 2022. Soil observations cover the period from 2001 to 2022, with steadily increasing sample
358 counts that peak in 2017 and 2022; 81% of these records include a collection date. Vegetation
359 observations had the longest temporal range, spanning from 1988 to 2020, with a prominent peak
360 in 2018. Nearly all vegetation observations (94%) are associated with a specific year. Water
361 observations were collected between 1991 and 2017, with a sharp spike in 2005 that far exceeds
362 sampling effort in other years. These records are the most complete in terms of temporal
363 metadata, with over 98% including a collection date.



364

365 **Figure 3.** 2D column chart showing the number of observations collected over time for (a) lake sediment,
366 (b) vegetation, (c) soil, and (d) water Hg observations in the PermHg database.

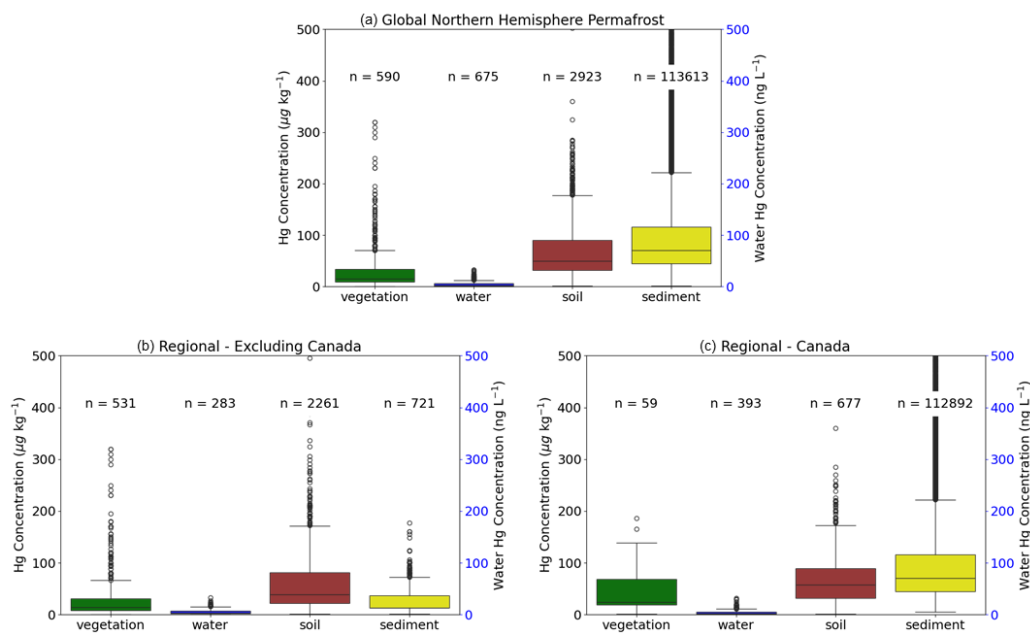
367

368 4.2. Data Analysis



369 Overall, the observation distribution is heavily biased by both matrix type and geographic
370 region. Lake sediment observations account for over 90% of all data points, highlighting a strong
371 skew toward this medium relative to soil, vegetation, and water. Geographically, the majority of
372 observations exist in Canada and across the Western Hemisphere, with Canada alone
373 contributing over 90% of the total observations. In contrast, there are significant spatial gaps in
374 Eurasia, particularly across Russia and northern China. This uneven distribution may reflect
375 differences in research funding, accessibility, existing monitoring programs, and the composition
376 of author teams. In addition, data availability may be limited in some countries where
377 observations are not routinely shared publicly or translated into English. As a result, care should
378 be taken when extrapolating trends across under-represented regions or observation types.

379 Boxplots were used to visualize Hg concentration distributions across lake sediment, soil,
380 vegetation, and water observations at both global and regional scales (**Fig. 4**). Across all subsets,
381 lake sediment exhibited the highest median concentrations, followed by soil, with vegetation
382 consistently showing the lowest values. Mercury concentrations in water are reported in ng L^{-1}
383 and are plotted on a secondary y-axis to account for the differing units, while concentrations in
384 sediment, soil, and vegetation are reported in ug kg^{-1} dry weight. Across both global and
385 Canadian subsets, Hg concentrations follow a consistent pattern by matrix: lake sediment > soil
386 > vegetation. In contrast, observations from all other countries followed the order soil > lake
387 sediment > vegetation, which may be a result of the reversal of sample size for lake sediment and
388 soil observations.



389

390 **Figure 4.** Boxplots of Hg concentrations across lake sediment, soil, vegetation and water observation
391 types for (a) Global Northern Hemisphere Permafrost, (b) Regional – Excluding Canada, and (c) Regional
392 – Canada. T-tests within each grouping showed statistically significant differences among most
393 observation types, except between vegetation and sediment for countries outside Canada. Water Hg
394 concentrations are shown on a separate y-axis due to differing units (ng L^{-1} vs. $\mu\text{g kg}^{-1}$ dry weight) and
395 are not directly comparable to the other matrices.

396 We used two sample t-tests to assess whether differences in Hg concentrations between pairs
397 of observation types were statistically significant, considering only two groups at a time.
398 Mercury concentrations across all observation types were positively skewed, with most values
399 being low to moderate in concentration and a small number of high values elevating the mean. F-
400 tests were first used to assess the equality of variances before choosing a two-sample t-test.
401 Variances were unequal for all comparisons except between vegetation and soil ($p=0.013$
402 globally; $p=0.071$ within Canadian observations), so Welch's t-test (assuming unequal variances)
403 was used in most cases. Both global and regional analyses revealed statistically significant
404 differences in Hg concentrations among observation types, with the exception noted above.
405 Overall, these results reinforce the general pattern of lake sediment > soil > vegetation,
406 consistent with findings from non-permafrost regions. This hierarchy is consistent with



407 observations from other landscape types (i.e., non-cold regions), suggesting that these
408 concentration patterns may reflect general biogeochemical processes rather than being unique to
409 permafrost-affected environments (Gworek et al., 2016, 2020).

410

411 5. Discussion

412 The PermHg database should be useful to a wide audience including researchers and
413 scientists, policymakers, regulators, environmental managers, educators, and the public. With
414 regard to scientific research, this database may be useful for a wide variety of studies including
415 environmental fate and transport, contaminant modeling, risk assessment, climate change
416 impacts, remote sensing, earth system modeling, ecotoxicology, and food web studies. Potential
417 applications include but are not limited to calibration and validation of atmospheric and
418 terrestrial models, future global Hg budget studies, identifying global trends and regional
419 hotspots, biogeochemical controls, and assessing human and ecosystem health risks from Hg
420 exposure pathways. The database is also recommended for use in spatial analysis by providing
421 empirical constraints for satellite-based observations and synthesis reviews to support integrated
422 Hg research in permafrost regions.

423 Outside of the scientific research community, this database can help assess whether Hg
424 concentrations exceed regional regulatory limits or advisories and support compliance with
425 international agreements like the Minamata Convention on Mercury. PermHg may aid in
426 identifying contaminated sites or regions needing additional intervention or monitoring and help
427 guide additional sampling or mitigation based on spatial and observation type gaps. The database
428 may also support baseline environmental studies for infrastructure development or resource
429 extraction. We hope this database will serve the public interest through real-world examples of
430 pollutant pathways and highlight global and local Hg concerns, especially in Arctic or
431 Indigenous communities where some country foods are at risk of elevated Hg concentrations
432 (Arctic Monitoring and Assessment Programme, 2022).

433 Due to methodological heterogeneity, the database has several limitations that should be
434 considered in future analysis and applications. These include uneven spatial and temporal
435 coverage, with sampling efforts concentrated in certain regions (e.g., Canada and the Western
436 Hemisphere) and time periods, leaving notable gaps in underrepresented areas such as Russia or



437 China. Temporal coverage of observations is sparse before the 1990s, and some observation
438 types include extended gaps in coverage (e.g., 3-5 years). A significant portion of the
439 measurements lack reported uncertainty or quality assurance information, limiting the ability to
440 assess data precision and comparability across studies. Variation in sampling methods, analytical
441 techniques, temporal heterogeneity in sampling period (e.g., day, month, season), and detection
442 limits may also contribute to inconsistencies and should be accounted for when interpreting or
443 modeling Hg in permafrost regions.

444 This database can serve as a valuable guide for research teams working in Arctic regions,
445 helping identify where new measurements could have the most impact and inform future field
446 collection efforts. As the first integrated Hg database for measurements in permafrost regions, it
447 provides a baseline for future observations and for tracking Hg levels and trends over time. To
448 support long-term growth and community engagement, the database is hosted on a GitHub
449 repository linked to Zenodo (see Sect. 5), enabling version-controlled contributions, transparent
450 issue tracking, and permanent archiving (concept DOI:10.5281/zenodo.18300989, Olson et al.,
451 2026). A contribution guide will provide instructions for submitting new data and ensuring
452 consistent quality control. Ongoing oversight could be coordinated through a lightweight
453 advisory mechanism, potentially under the International Permafrost Association or Arctic
454 Monitoring and Assessment Programme, to maintain data quality and guide updates. By
455 facilitating community-driven expansion in a structured, open-access format, the PermHg
456 database can contribute to international Hg monitoring efforts, including supporting
457 effectiveness evaluation under the Minamata Convention.

458 **6. Data Availability**

459 In alignment with open science principles, the PermHg dataset and its accompanying
460 documentation are hosted on GitHub (<https://github.com/IGE-mercury/PermHg>). The PermHg
461 database is archived on Zenodo under the concept DOI 10.5281/zenodo.18300989, which links
462 all released versions of the dataset. The specific version used and described in this manuscript is
463 archived as 10.5281/zenodo.18483492 (Olson et al., 2026). Users are encouraged to cite both this
464 data paper and the appropriate Zenodo DOI when using the dataset.

465 GitHub serves as the platform for community contributions and updates. Users who wish to
466 propose modifications, additions, or corrections to the data or documentation should follow the



467 contribution workflow outlined in the repository's README.md file. This involves creating a
468 personal copy of the repository, implementing changes, and submitting them for review via a
469 pull request. Once approved, changes are merged into the main branch, and periodic updates are
470 released on Zenodo to reflect significant additions or improvements.

471 For users unfamiliar with GitHub, data submissions are also welcome via email (permhg@univ-grenoble-alpes.fr). Our aim is to foster an open, evolving database that grows through
472 collaborative input, thereby supporting transparent and reproducible research.

474 A subset of the soil permafrost mercury observations included in the PermHg compilation ($n =$
475 1,752 records) originates from a curated permafrost mercury database hosted by the Bolin Centre
476 for Climate Research. These data are archived separately and will be cited via a dedicated digital
477 object identifier (DOI: XXX; a permanent DOI will be assigned upon acceptance/publication).

478 **7. Conclusion**

479 This study compiles one of the most comprehensive publicly available database of Hg
480 concentrations in permafrost-affected environments to date. PermHg addresses a longstanding
481 data gap of Hg concentrations in Arctic and sub-Arctic regions, allowing the opportunity to
482 analyze spatial patterns, assess climate change impacts, and model biogeochemical cycling at
483 regional to global scales. This database can inform monitoring programs, support regulatory
484 frameworks like the Minamata Convention, and guide international efforts to mitigate Hg
485 exposure in northern communities.

486 The development of this database was made possible through collaborative contributions
487 from a broad scientific community and is intended to support researchers, decision makers, and
488 the public. Its standardized format supports integration into Earth system models, remote
489 sensing products, and other geospatial datasets to track and predict Hg behavior in response to
490 environmental change. This database provides a critical foundation for future integrated Hg
491 research across high-latitude ecosystems.

492 The database is archived and accessible through a GitHub repository linked to Zenodo
493 (concept DOI:10.5281/zenodo.18300989), supporting continued development, citation, and reuse
494 (Olson et al., 2026). While current data coverage is uneven, PermHg highlights key areas where
495 future field sampling and monitoring could have the greatest impact, including Russia and China.



496 The incorporation of additional soil, vegetation, and water observations will also be essential to
497 providing a more balanced database across observation types. As permafrost regions continue to
498 warm, this database lays the foundation for more interdisciplinary investigations of Hg cycling
499 and implications to human and ecosystem health.

500 **8. Author contribution**

501 CLO, KS, AA, LT, and DO led the conceptualization of the study. CLO prepared the original
502 draft of the manuscript. All authors contributed data to the PermHg database and participated in
503 data curation and quality control. CLO and KS acquired financial support for the project. EJ,
504 CLO, and HA contributed to database curation, including preparation of metadata and uploading
505 data products to GitHub and Zenodo. All authors reviewed and edited the manuscript and
506 approved the final version.

507 **9. Competing Interests**

508 The authors declare that they have no conflict of interest.

509 **10. Acknowledgments**

510 Financial support for this work was provided by the International Permafrost Association Action
511 Group Award in 2024 ([https://www.permafrost.org/group/permhg-a-global-database-of-mercury-
512 concentrations-in-permafrost-and-active-layer-soils/](https://www.permafrost.org/group/permhg-a-global-database-of-mercury-concentrations-in-permafrost-and-active-layer-soils/)). LS, EJ, and HA received funding from the
513 ANR ATOX project (ANR-24-CE01-7616). The authors used ChatGPT (OpenAI, GPT-5-mini)
514 to assist with language editing and clarity of the manuscript. All scientific content,
515 interpretations, and data were authored and verified by the authors.

516

517 **11. References**

518 Basu, N., Abass, K., Dietz, R., Krümmel, E., Rautio, A., and Weihe, P.: The impact of mercury
519 contamination on human health in the Arctic: A state of the science review, *Science of The Total
520 Environment*, 831, 154793, <https://doi.org/10.1016/j.scitotenv.2022.154793>, 2022.

521 Chételat, J., McKinney, M. A., Amyot, M., Dastoor, A., Douglas, T. A., Heimbürger-Boavida,
522 L.-E., Kirk, J., Kahilainen, K. K., Outridge, P. M., Pelletier, N., Skov, H., St. Pierre, K.,
523 Vuorenmaa, J., and Wang, F.: Climate change and mercury in the Arctic: Abiotic interactions,
524 *Science of The Total Environment*, 824, 153715,
525 <https://doi.org/10.1016/j.scitotenv.2022.153715>, 2022.



- 526 Dastoor, A., Angot, H., Bieser, J., Christensen, J. H., Douglas, T. A., Heimbürger-Boavida, L.-
527 E., Jiskra, M., Mason, R. P., McLagan, D. S., Obrist, D., Outridge, P. M., Petrova, M. V.,
528 Ryjkov, A., St. Pierre, K. A., Schartup, A. T., Soerensen, A. L., Toyota, K., Travnikov, O.,
529 Wilson, S. J., and Zdanowicz, C.: Arctic mercury cycling, *Nature Reviews Earth &*
530 *Environment*, 3, 270–286, <https://doi.org/10.1038/s43017-022-00269-w>, 2022.
- 531 Fabre, C., Sonke, J. E., Tananaev, N., and Teisserenc, R.: Organic carbon and mercury exports
532 from pan-Arctic rivers in a thawing permafrost context – A review, *Science of The Total*
533 *Environment*, 954, 176713, <https://doi.org/10.1016/j.scitotenv.2024.176713>, 2024.
- 534 Gartler, S., Scheer, J., Meyer, A., Abass, K., Bartsch, A., Doloisio, N., Falardeau, J., Hugelius,
535 G., Irrgang, A., Haukur Ingimundarson, J., Jungsberg, L., Lantuit, H., Nymand Larsen, J., Lodi,
536 R., Martin, V. S., Mercer, L., Nielsen, D., Overduin, P., Povoroznyuk, O., Rautio, A.,
537 Schweitzer, P., Speetjens, N. J., Tomaškovičová, S., Timlin, U., Vanderlinden, J.-P., Vonk, J.,
538 Westerveld, L., and Ingeman-Nielsen, T.: A transdisciplinary, comparative analysis reveals key
539 risks from Arctic permafrost thaw, *Communications Earth & Environment*, 6, 21,
540 <https://doi.org/10.1038/s43247-024-01883-w>, 2025.
- 541 Giest, F. P., Jenrich, M., Grosse, G., Jones, B. M., Mangelsdorf, K., Windirsch, T., and Strauss,
542 J.: Organic carbon, mercury, and sediment characteristics along a land–shore transect in Arctic
543 Alaska., *Biogeosciences*, 22, 2871–2887, <https://doi.org/10.5194/bg-22-2871-2025>, 2025.
- 544 Gworek, B., Bemowska-Kalabun, O., Kijenska, M., and Wrzosek-Jakubowska, J.: Mercury in
545 Marine and Oceanic Waters—a Review, *WATER AIR AND SOIL POLLUTION*, 227,
546 <https://doi.org/10.1007/s11270-016-3060-3>, 2016.
- 547 Gworek, B., Dmuchowski, W., and Baczevska-Dąbrowska, A. H.: Mercury in the terrestrial
548 environment: a review, *Environmental Sciences Europe*, 32, 128, [https://doi.org/10.1186/s12302-](https://doi.org/10.1186/s12302-020-00401-x)
549 [020-00401-x](https://doi.org/10.1186/s12302-020-00401-x), 2020.
- 550 Horsburgh, J. S., Tarboton, D. G., Piasecki, M., Maidment, D. R., Zaslavsky, I., Valentine, D.,
551 and Whitenack, T.: An integrated system for publishing environmental observations data,
552 *Environmental Modelling & Software*, 24, 879–888,
553 <https://doi.org/10.1016/j.envsoft.2009.01.002>, 2009.
- 554 Jonsson, S., Mastromonaco, M. N., Wang, F., Bravo, A. G., Cairns, W. R. L., Chételat, J.,
555 Douglas, T. A., Lescord, G., Ukonmaanaho, L., and Heimbürger-Boavida, L.-E.: Arctic
556 methylmercury cycling, *Science of The Total Environment*, 850, 157445,
557 <https://doi.org/10.1016/j.scitotenv.2022.157445>, 2022.
- 558 Kang, H., Liu, X., Guo, J., Zhang, Q., Wang, Y., Huang, J., Xu, G., Wu, G., Ge, W., and Kang,
559 S.: Long-term mercury variations in tree rings of the permafrost forest, northeastern China, *Sci.*
560 *China Earth Sci.*, 65, 1328–1338, <https://doi.org/10.1007/s11430-021-9886-1>, 2022.
- 561 Lim, A. G., Jiskra, M., Sonke, J. E., Loiko, S. V., Kosykh, N., and Pokrovsky, O. S.: A revised
562 pan-Arctic permafrost soil Hg pool based on Western Siberian peat Hg and carbon observations.,
563 *Biogeosciences*, 17, 3083–3097, <https://doi.org/10.5194/bg-17-3083-2020>, 2020.



- 564 MacMillan, G. A., Girard, C., Chételat, J., Laurion, I., and Amyot, M.: High Methylmercury in
565 Arctic and Subarctic Ponds is Related to Nutrient Levels in the Warming Eastern Canadian
566 Arctic, *Environ. Sci. Technol.*, 49, 7743–7753, <https://doi.org/10.1021/acs.est.5b00763>, 2015.
- 567 Mei Lu, Wang Xun, Feng Xinbin, and Luo Ji: Spatial distribution and source/ sink characteristic
568 of mercury in the water samples from the Mt. Gongga area in the Tibetan Plateau, *Huanjing*
569 *Huaxue-Environmental Chemistry*, 35, 1549–1556, [https://doi.org/10.7524/j.issn.0254-](https://doi.org/10.7524/j.issn.0254-6108.2016.08.2015122301)
570 6108.2016.08.2015122301, 2016.
- 571 Obrist, D., Agnan, Y., Jiskra, M., Olson, C. L., Colegrove, D. P., Hueber, J., Moore, C. W.,
572 Sonke, J. E., and Helmig, D.: Tundra uptake of atmospheric elemental mercury drives Arctic
573 mercury pollution, *Nature*, 547, 201–204, <https://doi.org/10.1038/nature22997>, 2017.
- 574 Obu, J., Westermann, S., Bartsch, A., Berdnikov, N., Christiansen, H. H., Dashtseren, A.,
575 Delaloye, R., Elberling, B., Etzelmüller, B., Kholodov, A., Khomutov, A., Kääh, A., Leibman,
576 M. O., Lewkowicz, A. G., Panda, S. K., Romanovsky, V., Way, R. G., Westergaard-Nielsen, A.,
577 Wu, T., Yamkhin, J., and Zou, D.: Northern Hemisphere permafrost map based on TTOP
578 modelling for 2000–2016 at 1 km² scale, *Earth-science reviews*, 299–316, 2019a.
- 579 Obu, J., Westermann, S., Bartsch, A., Berdnikov, N., Christiansen, H., Dashtseren, A., Delaloye,
580 R., Elberling, B., Etzelmüller, B., Kholodov, A., Khomutov, A., Kääh, A., Leibman, M.,
581 Lewkowicz, A., Panda, S., Romanovsky, V., Way, R., Westergaard-Nielsen, A., Wu, T.,
582 Yamkhin, J., and Zou, D.: Northern Hemisphere permafrost map based on TTOP modelling for
583 2000-2016 at 1 km² scale, *EARTH-SCIENCE REVIEWS*, 193, 299–316,
584 <https://doi.org/10.1016/j.earscirev.2019.04.023>, 2019b.
- 585 Olson, C.I., Geyman, B., Thackray, C., Krabbenhoft, D., Tate, M., Sunderland, E., and Driscoll,
586 C.: Mercury in soils of the conterminous United States: patterns and pools, *ENVIRONMENTAL*
587 *RESEARCH LETTERS*, 17, <https://doi.org/10.1088/1748-9326/ac79c2>, 2022.
- 588 Olson, C., Jiskra, M., Biester, H., Chow, J., and Obrist, D.: Mercury in Active-Layer Tundra
589 Soils of Alaska: Concentrations, Pools, Origins, and Spatial Distribution, *Global Biogeochemical*
590 *Cycles*, 32, 1058–1073, <https://doi.org/10.1029/2017GB005840>, 2018.
- 591 Olson, C. L., Jiskra, M., Sonke, J. E., and Obrist, D.: Mercury in tundra vegetation of Alaska:
592 Spatial and temporal dynamics and stable isotope patterns, *Science of the total environment*,
593 1502–1512, 2019.
- 594 Olson, C., Schaefer, K., Azaroff, A., Angot, H., Douglas, T. A., Fahnestock, M. F., Haugk, C.,
595 Hugelius, G., Jahangir, E., Jonsson, S., Kirkwood, A., Korosi, J., Nasr, M., Olefeldt, D., Olson,
596 C., Sereni, L., Shakil, S., St. Pierre, K., Thompson, L., and Zolkos, S.: A Consolidated Database
597 of Mercury Observations for Permafrost Regions, 2026. <https://zenodo.org/records/18301176>
- 598 Outridge, P. M., Mason, R. P., Wang, F., Guerrero, S., and Heimbürger-Boavida, L. E.: Updated
599 Global and Oceanic Mercury Budgets for the United Nations Global Mercury Assessment 2018,
600 *Environ. Sci. Technol.*, 52, 11466–11477, <https://doi.org/10.1021/acs.est.8b01246>, 2018.



- 601 Schaefer, K., Elshorbany, Y., Jafarov, E., Schuster, P. F., Striegl, R. G., Wickland, K. P., and
602 Sunderland, E. M.: Potential impacts of mercury released from thawing permafrost, *Nature*
603 *Communications*, 11, 4650, <https://doi.org/10.1038/s41467-020-18398-5>, 2020.
- 604 Schuster, P. F., Schaefer, K. M., Aiken, G. R., Antweiler, R. C., Dewild, J. F., Gryzniec, J. D.,
605 Gusmeroli, A., Hugelius, G., Jafarov, E., Krabbenhoft, D. P., Liu, L., Herman-Mercer, N., Mu,
606 C., Roth, D. A., Schaefer, T., Striegl, R. G., Wickland, K. P., and Zhang, T.: Permafrost Stores a
607 Globally Significant Amount of Mercury, *Geophysical Research Letters*, 45, 1463–1471,
608 <https://doi.org/10.1002/2017GL075571>, 2018.
- 609 Sonke, J., Teisserenc, R., Heimbürger-Boavida, L., Petrova, M., Maruszczak, N., Le Dantec, T.,
610 Chupakov, A., Li, C., Thackray, C., Sunderland, E., Tananaev, N., and Pokrovsky, O.: Eurasian
611 river spring flood observations support net Arctic Ocean mercury export to the atmosphere and
612 Atlantic Ocean, *PROCEEDINGS OF THE NATIONAL ACADEMY OF SCIENCES OF THE*
613 *UNITED STATES OF AMERICA*, 115, E11586–E11594,
614 <https://doi.org/10.1073/pnas.1811957115>, 2018.
- 615 Sonke, J., Angot, H., Zhang, Y., Poulain, A., Björn, E., and Schartup, A.: Global change effects
616 on biogeochemical mercury cycling, *AMBIO*, <https://doi.org/10.1007/s13280-023-01855-y>,
617 2023.
- 618 St. Pierre, K. A., Zolkos, S., Shakil, S., Tank, S. E., St. Louis, V. L., and Kokelj, S. V.:
619 Unprecedented Increases in Total and Methyl Mercury Concentrations Downstream of
620 Retrogressive Thaw Slumps in the Western Canadian Arctic, *Environ. Sci. Technol.*, 52, 14099–
621 14109, <https://doi.org/10.1021/acs.est.8b05348>, 2018.
- 622 Thompson, L. M., Shewan, R., Mangal, V., Harris, L. I., Cheng, C. H., Braga, L. P. P.,
623 Kolmakova, O., Tanentzap, A. J., Knorr, K. H., Kuhn, M. A., Haugk, C., Azaroff, A., Jonsson,
624 S., St. Louis, V. L., Lehnher, I., Quinton, W. L., Sonnentag, O., & Olefeldt, D. (2025).
625 Production of Methylmercury in Peatlands Following Permafrost Thaw Increases along a
626 Trophic Gradient. *Environmental Science & Technology*, 59(36), 19457–19467. [https://doi-](https://doi-org.colorado.idm.oclc.org/10.1021/acs.est.5c04510)
627 [org.colorado.idm.oclc.org/10.1021/acs.est.5c04510](https://doi-org.colorado.idm.oclc.org/10.1021/acs.est.5c04510)
- 628 Varty, S., Lehnher, I., St. Pierre, K., Kirk, J., and Wisniewski, V.: Methylmercury Transport and
629 Fate Shows Strong Seasonal and Spatial Variability along a High Arctic Freshwater Hydrologic
630 Continuum, *Environ. Sci. Technol.*, 55, 331–340, <https://doi.org/10.1021/acs.est.0c05051>, 2021.
- 631 Virkkala, A., Natali, S., Rogers, B., Watts, J., Savage, K., Connon, S., Mauritz, M., Schuur, E.,
632 Peter, D., Minions, C., Nojeim, J., Commane, R., Emmerton, C., Goeckede, M., Helbig, M.,
633 Holl, D., Iwata, H., Kobayashi, H., Kolari, P., López-Blanco, E., Marushchak, M., Mastepanov,
634 M., Merbold, L., Parmentier, F., Peichl, M., Sachs, T., Sonnentag, O., Ueyama, M., Voigt, C.,
635 Aurela, M., Boike, J., Celis, G., Chae, N., Christensen, T., Bret-Harte, M., Dengel, S., Dolman,
636 H., Edgar, C., Elberling, B., Euskirchen, E., Grelle, A., Hatakka, J., Humphreys, E., Järveoja, J.,
637 Kotani, A., Kutzbach, L., Laurila, T., Lohila, A., Mammarella, I., Matsuura, Y., Meyer, G.,
638 Nilsson, M., Oberbauer, S., Park, S., Petrov, R., Prokushkin, A., Schulze, C., St Louis, V.,
639 Tuittila, E., Tuovinen, J., Quinton, W., Varlagin, A., Zona, D., and Zyryanov, V.: The ABCflux
640 database: Arctic-boreal CO₂ flux observations and ancillary information aggregated to monthly



- 641 time steps across terrestrial ecosystems, *EARTH SYSTEM SCIENCE DATA*, 14, 179–208,
642 <https://doi.org/10.5194/essd-14-179-2022>, 2022.
- 643 Wohlgenuth, L., Rautio, P., Ahrends, B., Russ, A., Vesterdal, L., Waldner, P., Timmermann, V.,
644 Eickenscheidt, N., Fürst, A., Greve, M., Roskams, P., Thimonier, A., Nicolas, M., Kowalska, A.,
645 Ingerslev, M., Merilä, P., Benham, S., Iacoban, C., Hoch, G., Alewell, C., and Jiskra, M.:
646 Physiological and climate controls on foliar mercury uptake by European tree species,
647 *Biogeosciences*, 19, 1335–1353, <https://doi.org/10.5194/bg-19-1335-2022>, 2022.
- 648 Zhang, L., Qian, J.-L., and Planas, D.: Mercury concentration in tree rings of black spruce (*Picea*
649 *mariana* Mill. B.S.P.) in boreal Quebec, Canada, *Water Air Soil Pollut*, 81, 163–173,
650 <https://doi.org/10.1007/BF00477263>, 1995.
- 651 Zhang, Y., Zhang, P., Song, Z., Huang, S., Yuan, T., Wu, P., Shah, V., Liu, M., Chen, L., Wang,
652 X., Zhou, J., and Agnan, Y.: An updated global mercury budget from a coupled atmosphere-
653 land-ocean model: 40% more re-emissions buffer the effect of primary emission reductions, *One*
654 *Earth*, 6, 316–325, <https://doi.org/10.1016/j.oneear.2023.02.004>, 2023.
- 655 Zolkos, S., Krabbenhoft, D. P., Suslova, A., Tank, S. E., McClelland, J. W., Spencer, R. G. M.,
656 Shiklomanov, A., Zhulidov, A. V., Gurtovaya, T., Zimov, N., Zimov, S., Mutter, E. A., Kutny,
657 L., Amos, E., and Holmes, R. M.: Mercury Export from Arctic Great Rivers, *Environmental*
658 *Science & Technology*, 54, 4140–4148, <https://doi.org/10.1021/acs.est.9b07145>, 2020.
- 659